Supported Excavations: Observational Method and Inverse Modeling

Richard J. Finno, M.ASCE,[1] and Michele Calvello[2]

Abstract: An inverse analysis procedure that uses construction monitoring data to update predictions of deformations for supported excavation systems is presented. The numerical procedure is used to optimize the finite element model of a 12.2-m-deep excavation through Chicago glacial clays by minimizing the errors between monitoring data and computed displacements. The field observations are obtained from inclinometer data that measured lateral movements of the soil behind the supporting walls on opposite sides of the excavation throughout construction. Five construction stages are defined for the inverse analysis. At every new construction stage, the inclinometer data relative to that stage are added to the observations already available to "recalibrate" the model of the excavation. The constitutive responses of the soils are represented by the hardening-soil (H-S) model. Of the six basic H-S input parameters, only one parameter per layer is optimized, while the other parameters are either kept constant or related to the updated value of the optimized parameter. The methodology is effectively used to recalibrate the model of the excavation at early construction stages, such that good "predictions" are made of the behavior of the soil at later stages.

DOI: 10.1061/(ASCE)1090-0241(2005)131:7(826)

CE Database subject headings: Excavation; Construction methods; Deformation; Clays; Cold region; Illinois.

Introduction

Many factors affect movements associated with excavations, including stratigraphy, soil properties, support system details, construction activities, contractual arrangements and workmanship. In practice, when designers are faced with an excavation where ground movements are a critical issue, they can base their estimate of movements on semiempirical methods based in part on past performance data (e.g., Goldberg et al. 1976; Mana and Clough 1981; Clough and O'Rourke 1990) or on results of finite element analyses made specifically for the project. A main limitation of the first approach is the variety of construction details inherent in the case studies used in developing the empirical methods. However, if the exact construction procedure is known, a finite element analysis allows an engineer to model all aspects of excavation that cause stress change in soil: Wall installation, dewatering, cycles of excavation, bracing and brace removal, surcharges, and preloading of anchors.

In recent years, numerical simulations have become much more common for the analysis of excavations in urban environments. Finite element predictions, however, contain uncertainties related to soil properties, support system details, and construction procedures. If one wants to predict and subsequently to evaluate the overall performance of a design, a procedure that incorporates an evaluation of the results of the analyses must be defined. The procedure to accomplish this task is usually referred to as the "observational method" (Peck 1969; Morgenstern 1995; Whitman 1996), a framework wherein construction and design procedures and details are adjusted based upon observations and measurements made as construction proceeds. While the observational method is conceptually very helpful, it is quite difficult to use observed movements for controlling construction in a timely enough fashion to be of use in a typical excavation project, where time is of the essence to a contractor, or to judge quantitatively how well the work is proceeding.

To provide a tool to improve the state-of-the-practice of controlling ground movements associated with supported excavations, this paper presents a numerical procedure for supported excavation in clays that effectively and efficiently updates design predictions of lateral deformations during construction. Inclinometer data are used as observations in an inverse analysis that calibrates the numerical model of the excavation and thus supports, in an objective way, the engineering judgments made during the construction of the excavation system. The inverse analysis methodology is developed and tested using data from a 12.2-m-deep excavation through soft clays in Chicago (Finno et al. 2002).

Inverse Modeling: Updating Design Predictions Using Field Observations

In model calibration, various parts of the model are changed so that the measured values are matched by equivalent computed values until the resulting calibrated model accurately represents the main aspects of the actual system. In practice, numerical models typically are calibrated using trial-and-error methods. Inverse analysis works in the same way as a nonautomated calibration approach: Parameter values and other aspects of the model are

[1]Professor, Dept. of Civil and Environmental Engineering, Northwestern Univ., Evanston, IL 60208. E-mail: r-finno@northwestern.edu

[2]Postdoctoral Scholar, Univ. della Basilicata, Potenza, Italy.

Note. Discussion open until December 1, 2005. Separate discussions must be submitted for individual papers. To extend the closing date by one month, a written request must be filed with the ASCE Managing Editor. The manuscript for this paper was submitted for review and possible publication on November 25, 2002; approved on November 1, 2004. This paper is part of the ***Journal of Geotechnical and Geoenvironmental Engineering***, Vol. 131, No. 7, July 1, 2005. ©ASCE, ISSN 1090-0241/2005/7-826–836/$25.00.

adjusted until the model's computed results match the observed behavior of the system. Despite their apparent utility, however, inverse models are used for this purpose much less than one would expect because, perhaps, of the difficulties of implementing an inverse analysis and the complexity of the simulated systems.

The use of an inverse model provides results and statistics that offer numerous advantages in model analysis and, in many instances, expedites the process of adjusting parameter values. The fundamental benefit of inverse modeling is its ability to automatically calculate parameter values that produce the best fit between the observed and computed results. Additional benefits include saving substantial time over traditional trial-and-error calibration methods, providing statistics that quantify the quality of calibration, data shortcomings, and reliability of parameter estimates and predictions. The main difficulties inherent to inverse modeling algorithms are complexity, nonuniqueness, and instability. The complexity of real nonlinear systems sometimes leads to problems of insensitivity when the observations do not contain enough information to support estimation of the parameters. Nonuniqueness may result when different combinations of parameter values match the observations equally well. Instability can occur when slight changes in model variables radically change the inverse model results. Although these potential difficulties make inverse models imperfect tools, recent works in related civil engineering fields (Keidser and Rosjberg 1991; Ou and Tang 1994; Poeter and Hill 1997) demonstrate that inverse modeling provides capabilities that significantly help modelers, even when the simulated systems are very complex.

In the work described herein, model calibration by inverse analysis is conducted using *UCODE* (Poeter and Hill 1998), a computer code designed to allow inverse modeling posed as a parameter estimation problem. *UCODE* was developed for ground-water models, but it can be effectively used in geotechnical modeling because it works with any application software that can be executed in a batch mode. Its model independency allows the chosen numerical code to be used as a separate entity wherein modifications only involve model input values. This is an important feature of *UCODE*, in that it allows one to develop a procedure that can be easily employed in practice and in which the engineer will not be asked to use a particular finite element code or inversion algorithm. Rather, macros can be written in a Windows environment to couple *UCODE* with any finite element software.

Fig. 1 shows a detailed flowchart of the parameter optimization algorithm used in *UCODE*. With the results of a finite element prediction in hand, the computed results are compared with field observations in terms of an objective function. In *UCODE*, the weighted least-squares objective function $S(b)$ is expressed as

$$S(b) = [y - y'(b)]^T \omega [y - y'(b)] = e^T \omega e \tag{1}$$

where b=vector containing values of the parameters to be estimated; y=vector of the observations being matched by the regression; $y'(b)$=vector of the computed values which correspond to observations; ω=weight matrix wherein the weight of every observation is taken as the inverse of its error variance; and e=vector of residuals. This function represents a quantitative measure of the accuracy of the predictions.

A sensitivity matrix, X, is then computed using a forward difference approximation based on the changes in the computed solution due to slight perturbations of the estimated parameter values. This step requires multiple runs of the finite element code.

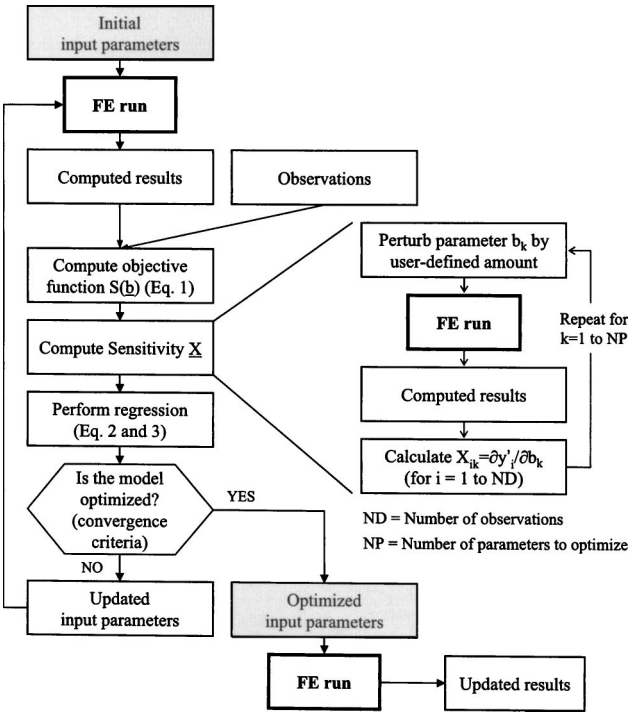

Fig. 1. Parameter optimization algorithm flowchart

Regression analysis of this nonlinear problem is used to find the values of the parameters that result in a best fit between the computed and observed values. In *UCODE*, this fitting is accomplished with the modified Gauss–Newton method, the results of which allow the parameters to be updated using

$$(C^T X^T r\omega X_r C + I m_r) C^{-1} d_r = C^T X^T r\omega (y - y'(b_r)) \tag{2}$$

$$b_{r+1} = \rho_r d_r + b_r \tag{3}$$

where d_r=vector used to update the parameter estimates b; r=parameter estimation iteration number; X_r=sensitivity matrix ($X_{ij}=\partial y_i/\partial b_j$) evaluated at parameter estimate b_r; C=diagonal scaling matrix with elements c_{jj} equal to $1/\sqrt{(X^T\omega X)_{jj}}$; I=identity matrix; m_r=Marquardt parameter (Marquardt 1963) used to improve regression performance; and ρ_r=damping parameter, computed as the change in consecutive estimates of a parameter normalized by its initial value, but it is restricted to values less than 0.5. The Marquardt parameter is initially set equal to 0 for each parameter estimation iteration r [see Eq. (3)]. For iterations in which the vector d defines parameter changes that are unlikely to reduce the value of the objective function, as determined by the Cooley and Naff (1990) condition, m_r is increased by $1.5m_{r(\text{old})}+0.001$ until the condition is no longer met.

At a given iteration, after performing the modified Gauss–Newton optimization, one decides whether the updated model is optimized according to either of two convergence criteria:

1. The maximum parameter change of a given iteration is less than a user-defined percentage of the value of the parameter at the previous iteration; or
2. The objective function, $S(b)$, changes less than a user-defined amount for three consecutive iterations.

After the model is optimized, the final set of input parameters is used to run the finite element model one last time and produce the "updated" prediction of future performance.

J. Geotech. Geoenviron. Eng., 2005, 131(7): 826-836

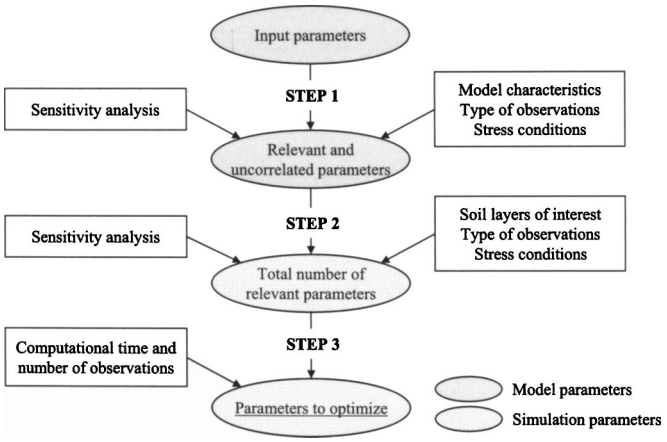

Fig. 2. Identification of soil parameters to optimize by inverse analysis

The relative importance of the input parameters being simultaneously estimated can be defined using various parameter statistics (Hill 1998). The statistics found most useful for this work are the composite scaled sensitivity, ccs_j, and the correlation coefficient, $\mathrm{cor}(i,j)$. The value of css_j indicates the total amount of information provided by the observations for the estimation of parameter j, and is defined as:

$$\mathrm{css}_j = \left[\sum_{j=1}^{ND} \left(\left(\frac{\partial y_i'}{\partial b_j} \right) b_j \omega_{ii}^{1/2} \right)^2 \Big|_b \Big/ ND \right]^{1/2} \tag{4}$$

where y_i'=ith computed value; b_j=jth estimated parameter; $\partial y_i / \partial b_j$=sensitivity of the ith computed value with respect to the jth parameter; ω_{jj}=weight of the ith observation; and ND=number of observations.

The values of $\mathrm{cor}(i,j)$ indicate the correlation between the ith and jth parameters, and are defined as

$$\mathrm{cor}(i,j) = \frac{\mathrm{cov}(i,j)}{\mathrm{var}(i)^{1/2}\mathrm{var}(j)^{1/2}} \tag{5}$$

where $\mathrm{cov}(i,j)$=off-diagonal elements of the variance-covariance matrix $V(b')=s^2(X^T\omega X)^{-1}$; s^2=model error variance; and $\mathrm{var}(i)$ and $\mathrm{var}(j)$ refer to the diagonal elements of $V(b')$.

Inverse analysis algorithms allow the simultaneous calibration of multiple input parameters. However, identifying the important parameters to include in the inverse analysis can be problematic, and it generally is not possible to use a regression analysis to estimate every input parameter of a given simulation. The number and type of input parameters that one can expect to estimate simultaneously depend on a number of factors, including the soil models used, the stress conditions of the simulated system, available observations, and numerical implementation issues. Note that within the context of finite element simulations, individual entries within element stiffness matrices may depend on combinations of soil parameters, implying that more than one combination of these parameters can yield the same result. Consequently, these parameters will be correlated within the context of the optimization solution, even though the parameters may be independent from a geotechnical perspective. Fig. 2 shows a procedural flowchart that can be used for the identification of the soil parameters to optimize by inverse analysis. The total number of input parameters can be reduced, in three steps, to the number of parameters that are likely to be optimized successfully by inverse analysis.

In Step 1, the number of relevant and uncorrelated parameters of the constitutive model chosen to simulate the soil behavior is determined. The number of parameters that can be estimated by inverse analysis depends upon the characteristics of the model, the type of observations available, and the stress conditions in the soil. Composite scaled sensitivity values [Eq. (4)] can provide valuable information on the relative importance of the different input parameters of a given model. Parameter correlation coefficients [Eq. (5)] can be used to evaluate which parameters are correlated and are, therefore, not likely to be estimated simultaneously by inverse analysis. In Step 2, the number of soil layers to calibrate and the type of soil model used to simulate the layers

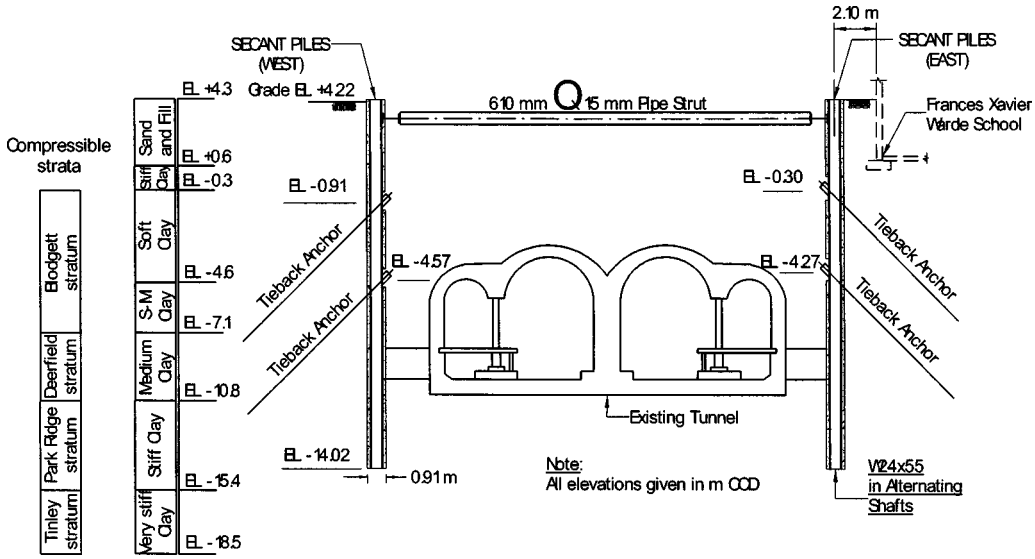

Fig. 3. Section view of excavation support system

J. Geotech. Geoenviron. Eng., 2005, 131(7): 826-836

determine the total number of relevant parameters of the simulation. An additional sensitivity analysis may be necessary to check for correlations between parameters relative to different layers. Finally, in Step 3, the total number of observations available and computational time considerations may prompt a final reduction of the number of parameters to optimize simultaneously. A detailed example of this procedure is presented by Calvello and Finno (2004).

Chicago and State Excavation Project

The proposed methodology was developed and tested using data from the excavation/renovation of the Chicago Ave. and State St. subway station in Chicago (Finno et al. 2002). The project included the excavation of 12.2 m of soft to medium clay within 2 m of a school supported on shallow foundations. Fig. 3 shows a section of the stratigraphy and the excavation support system. The support system consisted of a secant pile wall with three levels of support, which included pipe struts (first level) and tieback anchors (second and third levels). Ground and school movements were recorded during construction to monitor the effects of the excavation on the integrity of the school.

Lateral movements of the soil behind the secant pile wall were recorded using five inclinometers located around the site. Vertical movements were obtained from optical survey points located along the outside walls of the school, on the roof, and on eight interior columns. Measurements of the different instruments were taken before the installation of the wall, and at frequent intervals during construction. The observations for the inverse analysis described herein are derived from inclinometer data obtained on opposite sides of the excavation at five stages of construction.

Finite Element Procedures

The finite element software *PLAXIS* 7.11 (Brinkgreve and Vermeer 1998) was used to compute the response of the soil around the excavation. The problem was simulated assuming plane-strain conditions. The soil stratigraphy was assumed to be uniform across the site. Eight soil layers were considered: A fill layer overlaying a clay crust, a compressible clay deposit in which five distinct clay layers were modeled and a relatively incompressible hard silty clay stratum, locally known as hardpan. The side boundaries of the mesh (total size 183 m $\times$ 28.7 m) were established beyond the zone of influence of the settlements induced by the excavation (Caspe 1966; Hsieh and Ou 1998). The finite element mesh boundary conditions were set using horizontal restraints for the left and right boundaries and total restraints for the bottom boundary.

Calculation Steps

Table 1 shows calculation phases and the construction stages used in the finite element simulations. Note that the tunnel tubes and the school adjacent to the excavation were explicitly modeled in the finite element simulations to take into account the effect of their construction on the soil surrounding the excavation. Stages, 1–5 refer to the construction stages for which the computed results are compared to the field data in the inverse analysis procedure. *PLAXIS* employs a penalty formulation so that undrained conditions can be explicitly modeled. Construction phases not noted as "consolidation" in Table 1 were modeled as undrained.

Table 1. *PLAXIS* Calculation Phases and Construction Stages

	Calculation phase	Construction stage
	0	Initial conditions
	1 to 4	Tunnel construction (1940)
	5	Consolidation stage
	6 to 10	School construction (1960)
	11	Consolidation stage
Wall installation	12	Reset displacements
	13	Drill secant pile wall (1999)
	14	Pour concrete in piles—Stage 1
	15	Consolidation stage (20 days)
Excavation	16	Excavate (+2.75 m) and install strut—Stage 2
	17	Excavate (−0.9 m)
	18	Prestress first tiebacks—Stage 3
	19	Excavate (−4.6 m)
	20	Prestress second tiebacks—Stage 4
	21	Excavate (−7.9 m)—Stage 5

Consolidation stages were included after the tunnel, school, and wall installation calculation phases (Table 1) to permit excess pore water pressures to equilibrate. In *PLAXIS*, these stages are computed using Biot's approach. Secant pile wall installation in the field is a three-dimensional process. To simulate this construction in the plane-strain analysis, elements representing the wall were excavated and a hydrostatic pressure equivalent to a water level located at the ground surface was applied to the face of the resulting trench (Calculation Phase 13 in Table 1). After computing the movements associated with this process, the excavated elements were replaced by elements with the properties of the secant pile wall (Calculation Phase 14). Details about the definition of the finite element problem, the calculation phases, and the model parameters used in the simulation described herein can be found in Calvello (2002).

Soil Parameters

The soil model used to characterize the clays in the *PLAXIS* simulation of the excavation is the hardening-soil (H-S) model (Schanz et al. 1999). This effective stress model is formulated within the framework of elastoplasticity. Plastic strains are calculated assuming multisurface yield criteria. Isotropic hardening is assumed for both shear and volumetric strains. The flow rule is nonassociative for frictional shear hardening and associative for the volumetric cap.

Table 2 shows the initial values of the six basic H-S input parameters for the five clay layers that are calibrated by inverse analysis. These parameters are the friction angle, φ, cohesion, c, dilation angle, ϕ, the reference secant Young's modulus at the 50% stress level, E_{50}^{ref}, the reference oedometer tangent modulus, $E_{\text{oed}}^{\text{ref}}$, and the exponent m which relates reference moduli to the stress level dependent moduli (E representing E_{50}, E_{oed}, and E_{ur}:

$$E = E^{\text{ref}}\left(\frac{c\cot\phi - \sigma_3'}{c\cot\phi + p^{\text{ref}}}\right)^m \tag{6}$$

where p^{ref}=reference pressure equal to 100 stress units; and σ_3'=minor principal effective stress. Also shown in Table 2 are values of the reference unloading modulus, $E_{\text{ur}}^{\text{ref}}$, at-rest earth pressure coefficient, k_0, and the coefficient of permeability, k. Layers 1 to 5 refer to the Upper Blodgett, Lower Blodgett, Deerfield,

J. Geotech. Geoenviron. Eng., 2005, 131(7): 826-836

Table 2. Initial Values of Hardening-Soil (H-S) Parameters for the Clay Layers

Parameter	Layer 1	Layer 2	Layer 3	Layer 4	Layer 5
Φ (°)	23.4	23.4	25.6	32.8	32.8
c (kPa)	0.05	0.05	0.05	0.05	0.05
ψ (°)	0	0	0	0	0
E_{50}^{ref} (kPa)	226	288	288	413	619
E_{oed}^{ref} (kPa)	158	202	202	289	433
m	0.8	0.8	0.85	0.85	0.85
E_{ur}^{ref} (kPa)	678	864	864	1,239	1,857
k(m/day)	0.00009	0.00009	0.00009	0.00009	0.00009
$k_{0(NC)}$	0.6	0.6	0.57	0.46	0.46

Notes: The reference pressure is p^{ref}=100 psf=4.8 kPa; and the first six parameters are the basic H-S input parameters.

Park Ridge, and Tinley layers, respectively. The initial estimates of the input parameters for Layers 1 to 4 were based on triaxial test results using the approach described in Calvello and Finno (2002). Because few laboratory data existed for the very stiff Layer 5 soil and very small movements were observed in that stratum, the initial values of the parameters for Layer 5 were selected to minimize movements in that stratum.

Table 3 summarizes the parameters used to model the sand and fill layer and the structural elements of the excavation support system. The sand and fill layer was modeled as an elastoplastic Mohr–Coulomb material. Observations during excavation indicated that this material had substantial apparent cohesion. The secant pile wall consisted of overlapping 0.9-m-diameter 18.3-m-long drilled shafts installed with an overlap of 155 mm. The secant pile wall was modeled as a linear elastic material with a "composite" modulus calculated to account for the wide flange sections placed in alternating shafts. The top level of support consisted of 600-mm-diameter 16 mm thick cross-lot steel pipe struts horizontally spaced at 6.1 m. Tieback anchors were used for the second and third levels of support. The regroutable tiebacks were bundled steel tendons. The steel tendons consisted of four or five (for the east and west wall, respectively) 15-mm-steel strands. The tieback anchors were 150 mm in diameter and were installed at a 1.5-m-center-to-center spacing. The struts and tendons were modeled as two-node elastic spring elements with constant spring stiffness, EA. The grouted portion of the anchor the tiebacks was modeled as a line element with an axial stiffness EA and no bending stiffness. Interface elements were placed between the soil and structural elements, except for the cross-lot brace.

The input parameters optimized by inverse analysis were chosen following the procedure described in Fig. 2. Note that the first step of the procedure refers to the selection of the "model parameters" (e.g., H-S model) that are relevant to the problem under study, the last two steps refer to the selection of the total number of "simulation parameters" (e.g., five soil layers calibrated simultaneously) to optimize by inverse analysis.

A sensitivity analysis indicated that the model's relevant and uncorrelated parameters are E_{50}^{ref} and ϕ (Calvello and Finno 2004). Results were also sensitive to changes in values of parameter m. However, parameter m was not included in the regression because the values of the correlation coefficients [Eq. (5)] between parameters m and E_{50}^{ref} were very close to 1.0 at every layer, indicating that the two parameters were not likely to be simultaneously and uniquely optimized.

From a simulation perspective, the results of the sensitivity analysis indicated that the parameters that most influence the computed displacements are the ones relative to Layers 1, 3, and 4. However, when all relevant parameters (i.e., E_{50}^{ref} and ϕ for Layers 1, 3, and 4) were optimized simultaneously, the regression did not converge to meaningful estimates of the parameters (Calvello 2002). Whereas, when the failure parameters, ϕ, were kept constant at their initial estimates, and only the stiffness parameters, E_{50}^{ref}, were optimized, the calibration of the simulation was successful. Calvello and Finno (2003) showed that shear stress levels in the soil around the excavation were much less than those corresponding to failure for the great majority of the soil. This is indeed expected for excavation support systems that are designed to restrict adjacent ground movements to acceptably small levels, and hence one would expect the stiffness parameters to have a greater effect on the simulated results than failure parameters. Note that the large shear strain levels in Fig. 7 arise mostly from the simulation of the tunnel installation.

Table 4 shows the H-S parameters updated by the regression algorithm. Fifteen parameters (E_{50}^{ref}, E_{oed}^{ref}, and E_{ur}^{ref} at five clay layers) were updated at every iteration, but only three of them

Table 3. Properties of Nonoptimized Materials

Parameter	Sand and fill	Secant pile wall	Top cross lot brace	Tiebacks (east)	Tiebacks (west)	Grouted anchor
Φ (°)	35					
c (kPa)	20					
Ψ (°)	5					
E (kPa)	18,400	5.93×10^6				
ν	0.3	0.2				
k (m/day)	15					
EA (kN)/m			10,200	2,780	3,470	1,160

Notes: Sand and fill modeled as an elastoplastic Mohr–Coulomb material; secant pile wall modeled as a linear elastic material; braces and tiebacks modeled as bar elements; and blank spaces indicate parameters are not required for model.

Table 4. Parameters Updated by Inverse Analysis

Layer	Parameter optimized	Related parameters	
1	$E_1=E_{50(1)}^{ref}$	$E_{oed(1)}^{ref}=0.7\ E_1$	$E_{ur(1)}^{ref}=3\ E_1$
2	$E_2=E_{50(2)}^{ref}=E_1$	$E_{oed(2)}^{ref}=0.7\ E_2$	$E_{ur(2)}^{ref}=3\ E_2$
3	$E_3=E_{50}^{ref}$	$E_{oed(3)}^{ref}=0.7\ E_3$	$E_{ur(3)}^{ref}=3\ E_3$
4	$E_4=E_{50}^{ref}$	$E_{oed(4)}^{ref}=0.7\ E_4$	$E_{ur(4)}^{ref}=3\ E_4$
5	$E_5=E_{50(5)}^{ref}=1.5\ E_4$	$E_{oed(5)}^{ref}=0.7\ E_5$	$E_{ur(5)}^{ref}=3\ E_5$

(E_1, E_3, and E_4) were directly estimated by the optimization algorithm. Parameter E_{50}^{ref} was chosen to "represent" the stiffness of the H-S model because changes in E_{50}^{ref} values also produce changes in the values of parameters E_{oed}^{ref} (equal to 0.7 times E_{50}^{ref}) and E_{ur}^{ref} (equal to three times E_{50}^{ref}), thus its calibration can be considered as "representative" of the calibration of all H-S stiffness parameters. The values of E_{oed}^{ref}, E_{50}^{ref}, E_{ur}^{ref}, ν_{ur}, and k_0 are interrelated in the hardening soil model. During input, *PLAXIS* checks the value of E_{oed}^{ref} for the given combination of parameters, and if it falls out of a realistic limit, it rejects the value and automatically assigns the nearest realistic value. This makes it impossible to use E_{oed}^{ref} in the optimization scheme because it can be changed internally—and hence outside the control of the inverse technique (Calvello 2002; Cavello and Finno 2004). The stiffness parameters at Layer 2 were assumed to be the same as those of Layer 1, parameter E_5 was assumed to be 1.5 times E_4 and the values of E_{oed}^{ref} were related, at every layer, to the updated values of E_{50}^{ref}. As shown in Fig. 3, Layers 1 and 2 are within the same geologic stratum, so there is a physical basis for representing these two strata with the same material properties. The values of the other parameters were kept constant at their initial estimates (Table 2). Note that changing the values of E_{50}^{ref} is not the same as merely changing the elastic parameters of an elastoplastic or linear elastic soil model because the hardening soil responses are nonlinear below the cap and the stiffness depends on more than E_{50}^{ref}.

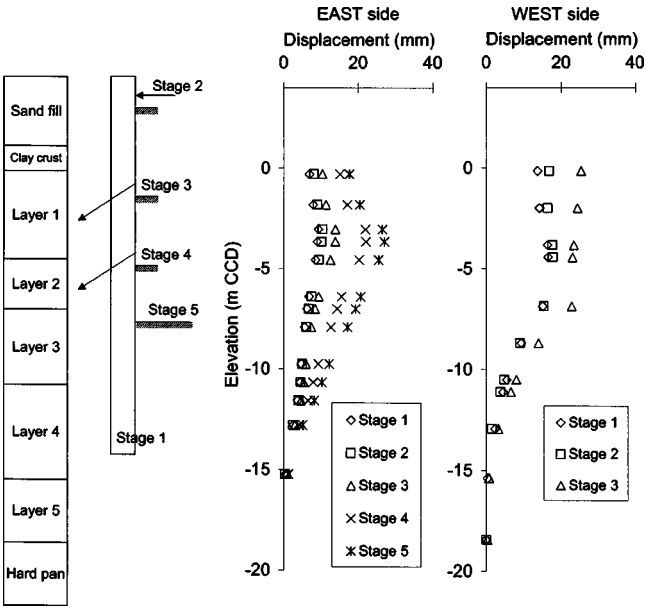

Fig. 4. Schematic of retaining system and observations points used from inclinometer readings

Observations and Weighting

Observations from inclinometers on both sides of the excavation were used to compare field data and computed displacements. Fig. 4 shows the observation points retrieved from the inclinometer readings for the five construction stages considered (Table 1). The soil profile and a schematic of the support system are also shown in the figure. Inclinometer readings were taken in the field every two feet. Not every reading, however, could be used as an observation for the inverse analysis because the finite element displacements were computed only at the intersection between the finite element mesh and the inclinometer location. Thus, 13 observation points were used for the east side and 11 observation points for the west side. The observations for the last two stages on the west side are not reported because the inclinometer was destroyed by construction activities after Stage 3.

One also could have used the settlement data with the inclinometer data to optimize the parameters. However, the H-S soil model, or for that matter, common commercially available models, cannot accurately predict the variation of settlements behind a wall because the transition from a "dynamic" stifffness at very small strains (less than 0.001%) to a value more typically found in triaxial tests (say 0.1% or greater), as well as their variation with direction of loading at these strain levels, are not included in the model. These stiffness variations are important in this type of problem because the strain levels vary from relatively high—very close to the wall—to zero—at some distance from the wall. Correct responses at the very small strain levels are required to obtain the correct settlement distributions. Optimization cannot overcome the limitations of a constitutive model, and hence only the lateral movements of the wall are used to calibrate the H-S model.

The inverse of the variance of the measurement errors was used to assign weights to the observations (i.e., inclinometer data). Based on the manufacturer's specification for accuracy of the inclinometer probe, the system accuracy, A, can be expressed as the lateral deviation over a given length of casing, in this case 0.025%. The measurement error of the inclinometer data increases as the distance increases from the bottom of the casing. Assuming that the error represents the 95% confidence interval of the measure, the weight for each point was computed from

$$\omega = \frac{1}{\sigma^2} = \frac{1}{\left(\frac{Ad/30.49}{1.96}\right)^2} \tag{7}$$

where σ=standard deviation; and d=distance from the bottom of the inclinometer casing in meters.

Results

Visual examination of the horizontal displacement distributions at the inclinometer locations provides the simplest way to evaluate the fit between computed and measured field response. Fig. 5 shows the comparison between the measured field data and the computed horizontal displacements when the initial estimates of the parameters are used. The comparison shows that the finite element model computes significantly larger displacements at every construction stage. The maximum computed horizontal displacements are about two times the measured ones and the computed displacement profiles result in significant and unrealistic movements in the lower clay layers. Results indicate that the stiffness properties for the clay layers based on laboratory data were less than field values.

J. Geotech. Geoenviron. Eng., 2005, 131(7): 826-836

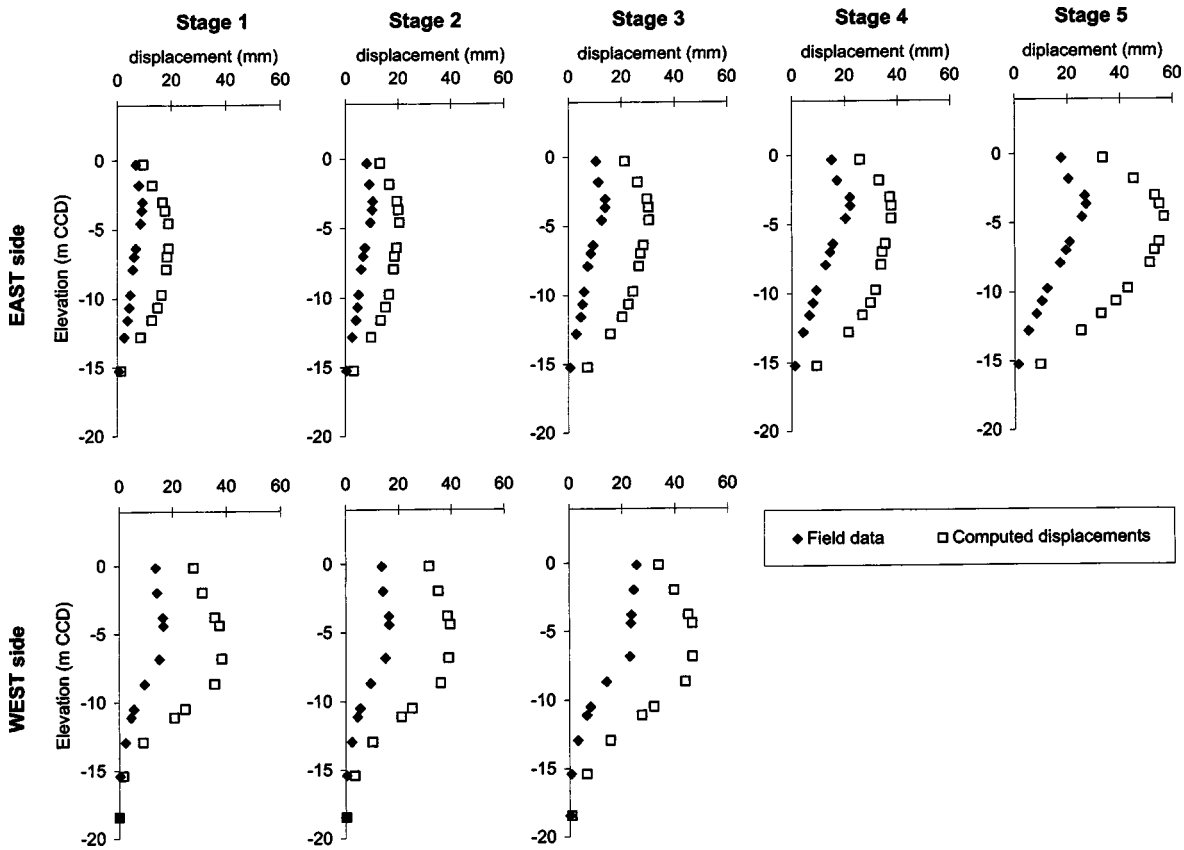

Fig. 5. Measured versus computed horizontal displacements: initial estimates of parameters

Fig. 6 shows the comparison between the measured field data and the computed horizontal displacements when parameters are optimized based on Stage 1 observations. The improvement of the fit between the computed and measured response is significant. Despite the fact that the optimized set of parameters is calculated using only Stage 1 observations, the positive influence on the calculated response is substantial for all construction stages. At the end of the construction (i.e., Stage 5) the maximum computed displacement exceeds the measured data by only about 15%. These results are significant in that a successful recalibration of the model at an early construction stage positively affects subsequent "predictions" of the soil behavior throughout construction.

Fig. 7 shows contours of equivalent shear strain computed after Stage 1, i.e., after the wall was installed (calculation step 14 in Table 1). The shear strains were as large as 5% in the clay layers that were optimized. These strains are large enough that significant nonlinearities developed even at the first optimization stage. These strains were sufficient to "exercise" the model so that the parameters could be optimized. Also note that the strains were less than 1% in most of the clay behind the wall, emphasizing the need to account for small strain stiffness variations when computing settlement distributions behind a wall.

Analyses were also made wherein parameters were recalibrated at every stage until the final construction stage (Stage 5). At every new construction stage, the inclinometer data relative to that stage were added to the observations already available. Fig. 8 shows the comparison between experimental and computed results when all observations are used to optimize the input parameters. Note that the final fit between the field and the computed results improves, especially in the upper soil layer. However, the difference with the fit shown in Fig. 6 is not significant because the inverse analysis performed after the first construction stage "recalibrated" the model parameters in such a way that the main behavior of the soil layers could be accurately predicted throughout construction.

Model Statistics

The inverse analysis procedure produces important byproducts that allow one to quantify the effectiveness of the optimization procedure and assess the reliability of the predictions. The *relative fit improvement*, RFI_i, which indicates by what percentage the optimized results improved compared to the predictions at the beginning of stage i, is defined as

$$\mathrm{RFI}_i = \frac{S(b)_{\mathrm{in}\_i} - S(b)_{\mathrm{fin}\_i}}{S(b)_{\mathrm{in}\_i}} \tag{8}$$

where $S(b)_{\mathrm{in}\_i}$-initial value of the objective function at stage i; and $S(b)_{\mathrm{fin}\_i}$-optimized value of the objective function at the end of stage i.

The *error variance*, s^2, a commonly used indicator of the overall magnitude of the weighted residuals, is computed as

$$s^2 = \frac{S(b)}{ND - NP} \tag{9}$$

where $S(b)$=objective function; ND=number of observations; and NP=number of estimated parameters.

At Stage 1, the reduction of the value of the initial objective function [Eq. (1)] of 2,132 to a value of 7.6 after optimization shows that the calibration of the finite element simulation—by inverse analysis based on the Stage 1 observations—is extremely

J. Geotech. Geoenviron. Eng., 2005, 131(7): 826-836

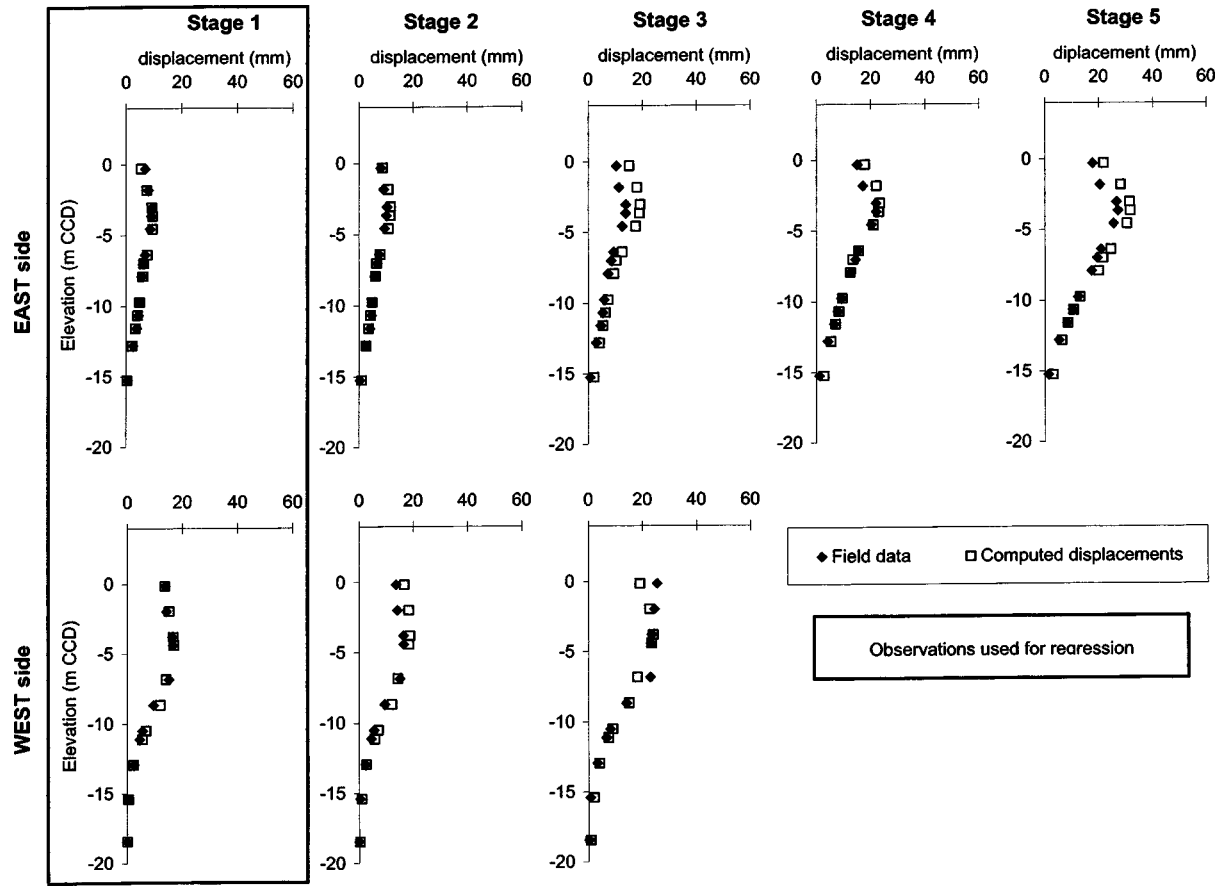

Fig. 6. Measured versus computed horizontal displacements: parameters optimized based on Stage 1 observations

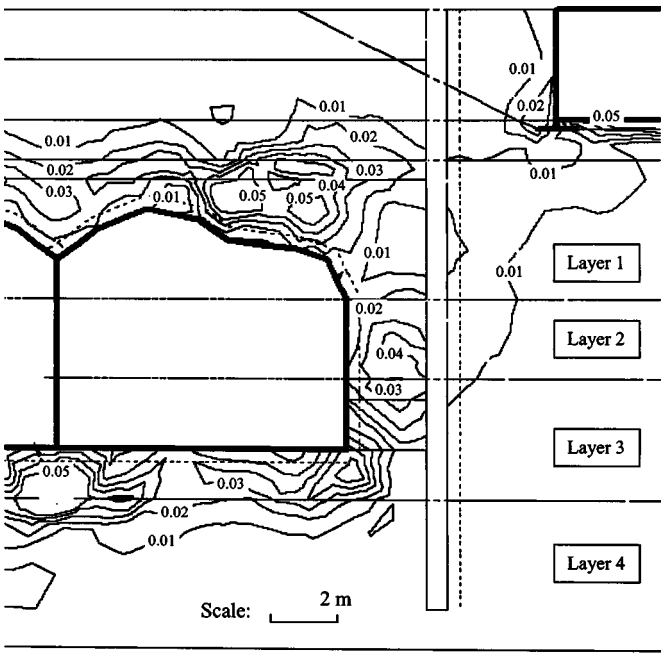

Strain contour interval = 0.01

Fig. 7. Computed shear strain contours: Stage 1

effective. The RFI value [Eq. (8)] indicates that the optimized results at Stage 1 improved by more than 99% compared to the initial predictions. The value of 0.40 of the model error variance, s^2 [Eq. (9)], which can be used to evaluate the consistency between the model fit and the measurement errors (Hill 1998), indicates that the fit is consistent with the weighting of the observations ($s^2 < 1.0$), and thus with the measurement errors associated with the inclinometer data.

The finite element model of the excavation was recalibrated at every construction stage. Fig. 9 shows the base and the final values of the error variance, s^2, at the various stages. The graph allows one to compare the overall magnitude of weighted residuals relative to the initial estimates of the parameters with the fit resulting from the calibrated models. Results show that error variance values decrease by more than two orders of magnitude at every stage. This indicates a significant improvement in the fit between observed and computed displacements. In all cases, the final error variance values are close to 1.0, indicating that the computed differences are consistent with the measurement errors.

Fig. 10 shows the values of relative fit improvement, RFI, at all stages and the values of the initial and final objective functions from which they are computed. Results show that Stage 1 observations improved the predictions by two orders of magnitude (i.e., RFI higher than 99%) and that, by the end of Stage 3, the recalibration of the model is essentially complete. These results are extremely promising because they indicate that early stage observations are able to recalibrate the finite element simulation in a way that is beneficial to the predictions of movements at later stages. One should note that, in this case, the early stage of construction refers to the installation of a secant pile wall that in-

J. Geotech. Geoenviron. Eng., 2005, 131(7): 826-836

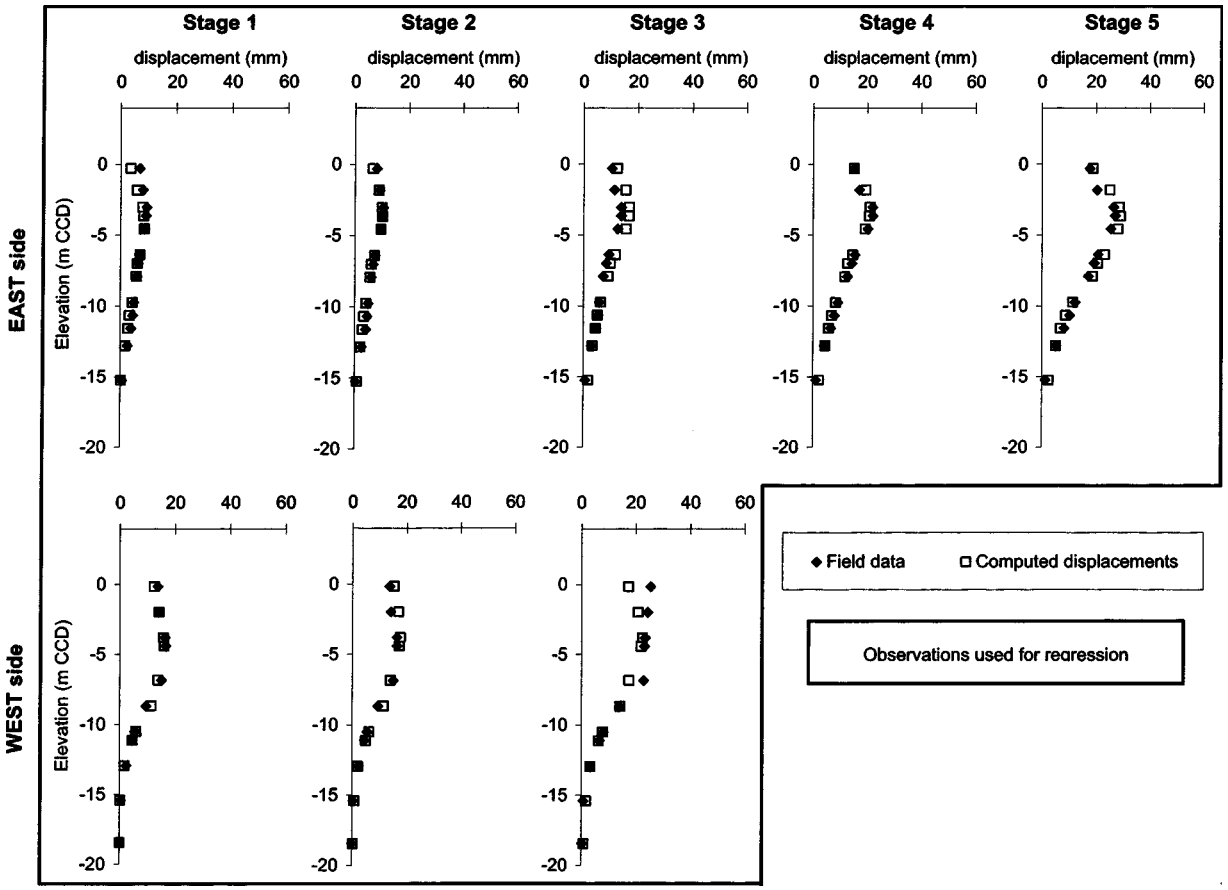

Fig. 8. Measured versus computed horizontal displacements: parameters optimized using all observations

duced movements throughout the compressible clay layers. These movements were large enough to exercise the models that represented responses of the soil most affected by the excavation.

Optimized Soil Parameters

Fig. 11 shows the initial and optimized values of the five input parameters at the different optimization stages. The variation of the input parameters at the five optimization stages is shown above a bar chart, representing the progress of the excavation, in which the excavation depth is normalized with respect to the excavation width. Results show that the maximum changes in parameter values occur at Stage 1, when the observations relative to the installation of the secant pile wall are used.

The results presented in Fig. 11 indicate that the initial estimates of the stiffness parameters are significantly lower than the optimized values of the parameters. This trend could be expected because the initial values were based on results of triaxial compression tests on specimens taken from thin-wall tubes. Note that if one was to arbitrarily increase the initial stiffness parameters prior to optimization, since one expects these values to be low, the magnitude of the increase is a matter of much judgment and would likely require adjustments to provide good fits to the observed data. The fact that initial parameters based on the laboratory data led to optimized parameters that resulted in a good fit, and made sense from a geotechnical viewpoint, illustrate the utility of the method.

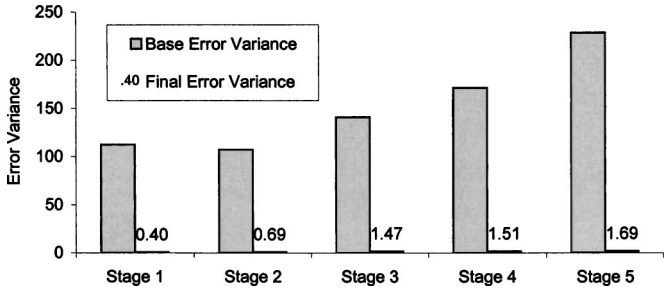

Fig. 9. Error variance values at each optimization stage

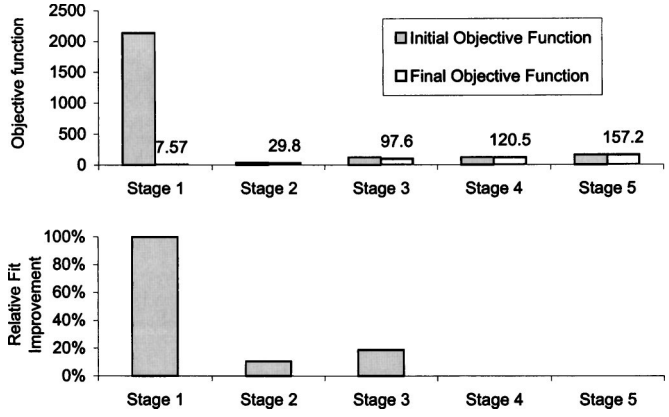

Fig. 10. Objective function and relative fit improvement values

J. Geotech. Geoenviron. Eng., 2005, 131(7): 826-836

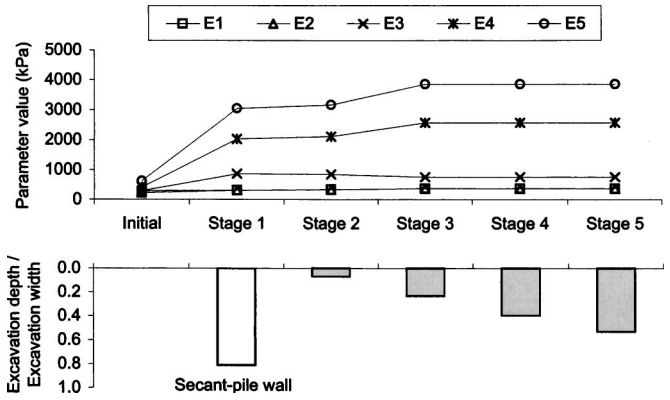

Fig. 11. Best-fit parameter values and normalized excavation depth at different optimization stages

As implied in Fig. 11, portions of the increase in optimized stiffness between Stages 2 and 3 may be a result of end effects of the excavation. The simulated excavation is really a three-dimensional problem modeled in plane strain. When the excavated depth is small, most of the wall can be adequately modeled as plane strain and, hence, little changes in parameters are noted between Stage 1 and 2. As the excavation deepens (Stage 3), the ratio between excavation depth and excavation width increases and higher parameter values compensate for the lack of constraints in the out-of-plane direction.

The H-S stiffness parameters are defined with respect to a reference pressure (p_{ref}=100 stress units). Thus, one cannot relate the values of E_{50}^{ref} directly to "typical" geotechnical estimates of moduli, but rather one must use Eq. (6). The parameter E_{50} represents a drained modulus. Nonetheless, the ratio E_{50}/S_u, where S_u is the undrained shear strength of the soil layer, can be used to judge the relative inherent stiffness of the various layers in undrained conditions. To compare the optimized values of the normalized stiffnesses of different layers, one has to consider the effective stresses of the soil. In Fig. 12, the E_{50}/S_u ratios are plotted as a function of S_u/σ_v', where σ_v' is the vertical effective stress at the start of the excavation. The σ_v' values refer to the stress conditions in the middle of the five clay layers on both sides of the excavation. The S_u values were based on field vane results from the Chicago-State site supplemented by site-specific water content data used in undrained strength correlations developed for Chicago glacial clays (Chung and Finno 1992). Results show that the ratio E_{50}/S_u increases linearly with S_u/σ_v'. The following expression describes the trend:

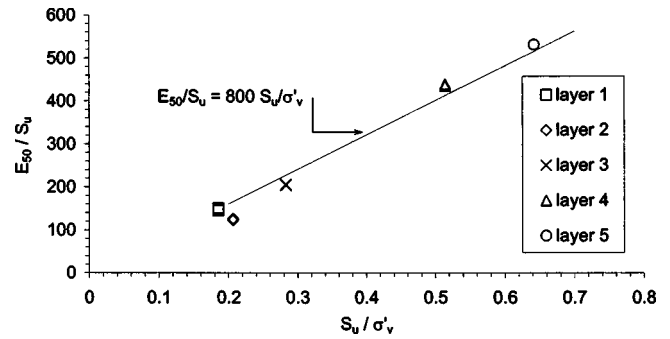

Fig. 12. E_{50}/S_u versus S_u/σ_1' for clay layers calibrated by inverse analysis

$$\frac{E_{50}}{S_u} = 800\frac{S_u}{\sigma_v'} \tag{10}$$

For Chicago glacial clays, Eqs. (6) and (10) can be conveniently used to compute the value of E_{50}^{ref} from estimates of S_u and σ_v', and parameters m, c, and φ, which are readily estimated.

While the statistics presented in this paper are useful in helping one to select parameters for optimization, engineering judgment is required to successfully apply the approach to a specific project. For example, if larger movements developed at the site, then perhaps parameters other than the stiffness would need to be optimized.

Conclusions

Based on results of the numerical analyses and comparisons with field performance data presented herein, the following conclusions can be drawn.

1. An inverse analysis procedure based on the integration of two commercially available software packages, used in conjunction with field observations of performance, was effectively used to update predictions of lateral movements at the excavation for the Chicago-State subway renovation.
2. When monitoring data—relative to the first construction stage (i.e., installation of the wall)—were used, the recalibrated model was able to "adequately" predict the behavior of the soil for all remaining construction stages. These results are significant in that a successful recalibration of the model at an early construction stage positively affects the predictions of the soil behavior throughout construction.
3. The objective function and relative fit improvement are statistics that were effective in quantifying the increased accuracy of the computed results.
4. The best-fit values of the stiffness parameters of the clay layers optimized in the analysis are significantly higher than the initial estimates of the parameters based on results of triaxial compression tests.
5. The optimized values of the stiffness parameters used herein were related to the ratio of the undrained shear strength to the initial vertical effective stress.

Acknowledgments

This work was funded by funds from grants CMS-0084664 and CMS-115213 from the National Science Foundation (NSF). The junior writer was partially supported by a grant from the Infrastructure Technology Institute (ITI) at Northwestern University. The writers thank Dr. Richard Fragaszy, Program Manager of Geomechanics and Geotechnical Systems at NSF and Mr. David Schulz, director of ITI, for their support.

References

Brinkgreve R. B. J., and Vermeer P. A. (1998). *Finite element code for soil and rock Analysis. PLAXIS 7.0 manual*, Balkema, Rotterdam, The Netherlands.

Calvello, M. (2002). "Inverse analysis of supported excavations through Chicago glacial clays." PhD thesis, Northwestern Univ., Evanston, Ill.

Calvello, M, and Finno R. J. (2002). "Calibration of soil models by inverse analysis." *Proc., Int. Symposium on Numerical Models in Geo-*

J. Geotech. Geoenviron. Eng., 2005, 131(7): 826-836

mechanics, NUMOG VIII, Balkema, Rotterdam, The Netherlands, 107–116.
Calvello, M., and Finno, R. J. (2003). "Modeling excavations in urban areas: Effects of past activities." *Ital. Geotech. J.*, 37(4), 9–23.
Calvello, M., and Finno, R. J. (2004). "Selecting parameters to optimize in model calibration by inverse analysis." *Comput. Geotech.*, 31(5), 411–425.
Caspe M. S. (1966). "Surface settlement adjacent to braced open cuts." *J. Soil Mech. Found. Div.*, 92, 51–59.
Chung, C. K., and Finno R. J. (1992). "Influence of depositional processes on the geotechnical parameters of Chicago glacial clays." *Eng. Geol. (Amsterdam)*, 32, 225–242.
Clough, G. W., and O'Rourke, T. D. (1990). "Construction induced movements of in situ walls." *Proc., Conf. on Design and Performance of Earth Retaining Structures*, ASCE, Geotechnical Special Publication No. 25, ASCE, New York, 439–470.
Cooley, R. L., and Naff, R. L. (1990). "Regression modeling of groundwater flow." *US Geological Survey techniques in water resources investigations*, USGS, Book 3, Chapter B4, 71–72.
Finno, R. J., Bryson, L. S., and Calvello, M. (2002). "Performance of a stiff support system in soft clay." *J. Geotech. Geoenviron. Eng.*, 128(8), 660–671.
Goldberg, D. T., Jaworski, W. E., and Gordon, M. D. (1976). "Lateral support systems and underpinning." Vol. 1 Design and Construction, *FHWA-RD-75-128*, Federal Highway Administration, Washington, D.C.
Hill, M. C. (1998). "Methods and guidelines for effective model calibration." U.S. Geological Survey Water-Resources investigations, *Rep. 98-4005*, USGS, 90.
Hsieh, P. G., and Ou C. Y. (1998). "Shape of ground surface settlement profiles caused by excavation." *Can. Geotech. J.*, 35, 1004–1017.
Keidser, A., and Rosjberg, D. (1991). "A comparison of four inverse approaches to groundwater flow and transport parameter identification." *Water Resour. Res.*, 27 (9), 2219–2232.
Mana, A. I., and Cough, G. W. (1981). "Prediction of movements for braced cuts in clay." *J. Geotech. Eng. Div., Am. Soc. Civ. Eng.*, 107(8), 759–777.
Marquardt, D. W. (1963). "An algorithm for least-squares estimation of nonlinear parameters." *J. Soc. Ind. Appl. Math.*, 11(8), 431–441.
Morgenstern, N. (1995). "Managing risk in geotechnical engineering." *Proc., 10th Pan American Conf. on Soil Mechanics and Foundation Engineering*, Vol. 4.
Ou, C. Y., and Tang Y. G. (1994). "Soil parameter determination for deep excavation analysis by optimization." *J. Chin. Inst. Eng.*, 17(5), 671–688.
Peck, R. B. (1969). "Deep excavations and tunneling in soft ground." *Proc., 7th Int. Conf. on Soil Mechanics and Foundation Engineering*, State-of-the-Art Volume, 225–290.
Poeter, E. P., and Hill, M. C. (1997). "Inverse methods: A necessary next step in groundwater modeling." *Ground Water*, 35(2), 250–260.
Poeter, E. P., and Hill, M. C. (1998). "Documentation of *UCODE*, a computer code for universal inverse modeling." U.S. Geological Survey Water-Resources investigations *Rep. No. 98-4080*, USGS,
Schanz, T., Vermeer, P. A., and Bonnier, P. G. (1999). "The hardening soil model—formulation and verification." *Proc., Plaxis Symposium Beyond 2000 in Computational Geotechnics*, Balkema, Amsterdam, The Netherlands, 281–296.
Whitman, R. V. (2000). "Organizing and evaluating uncertainty in geotechnical engineering." *J. Geotech. Geoenviron. Eng.*, 126(7), 583–593.

J. Geotech. Geoenviron. Eng., 2005, 131(7): 826-836